Thermal Conductivity of ice polymorphs: a computational study

Irene Iriarte-Carretero,[a] Miguel A. Gonzalez,[*a,‡] and Fernando Bresme[*a]

Thermal transport in ice features an unusual response. In addition to its intrinsic scientific interest, an understanding of the mechanisms determining the thermal conductivity of ice might be relevant in climate modelling and planetary science. Accurate microscopic models can provide important molecular insight into these mechanisms. In this work, we quantify using molecular simulations and state of the art forcefields, the thermal conductivity of ice Ih, VI, VII and a plastic phase that has been proposed very recently at pressures in the GPa range. The TIP4P models used in this study underestimate significantly the thermal conductivity of ice Ih and ice VII, while they show good agreement with experimental measurements of ice VI. The discrepancies observed are examined by investigating the temperature dependence of the thermal conductivity. The simulations indicate that the models are too anharmonic and they potentially feature a higher structural disorder than the experimental systems. We suggest that at high pressures the simulated thermal conductivities can be rationalized in terms of the performance of the models in predicting the equation of state of ice. The thermal conductivity of the plastic phase is very similar to that of the coexisting ice VII. Since the water molecules in the plastic phase feature orientational disorder, these results indicate that the hydrogen bond network does not play a significant role in defining the thermal transport mechanisms of ice at high pressures.

1 Introduction

Water is the most abundant substance on the surface of the Earth. Being an efficient fluid at regulating temperature and transporting heat, it is key at enabling biological processes[1] and of practical use in thermal management problems in industry[2]. The thermal properties of liquid water have been investigated extensively. It is well established that the thermal conductivity of water features an anomalous behaviour[3], and it is unusually high, > 0.5 mW/(K m)[4–8]. The anomalous behaviour of water has often been interpreted in terms of the hydrogen bonding structure[4]. The behaviour of water away from equilibrium is also unusual. It was shown recently that thermal gradients polarize water[9]. This effect is expected to be particularly relevant near critical conditions[10].

The solid phase of water, hexagonal ice (Ih), is the most abundant phase, and it is stable at standard pressure. This phase takes part in the regulation of the global climate by modifying the albedo and the adsorption of sunlight. Water features a very complex phase diagram with many ice polymorphs[3]. A number of high pressure phases (MPa-GPa range), which might be relevant in the geophysics of planetary interiors, have been uncovered too. Recent computer simulations focused on the refinement of simulation models to reproduce the experimental phase diagram of ice[11,12]. It was shown that the models provide a good account of the general phase behaviour of ice, and a new plastic phases was predicted at high pressures (GPa) and temperatures (>400 K)[13].

Experiments have revealed an unusual dependence of the thermal conductivity with pressure, which, unlike in most solids, decreases with pressure for ice Ih[14]. The thermal conductivity of high pressures phases, ice VI and VII at >1 GPa has also been measured[15]. More recently, it was shown that the thermal conductivity of ice VII can be very high, ~ 25 W K^{-1} m^{-1}, at high pressures, 22 GPa[16]. While the thermal conductivity of liquid water has been investigated in a number of theoretical studies (see[6,7,14] and references therein), less work has been devoted to study the thermal conduction of ice[17,18]. However, there are no theoretical studies of high pressures phases, ice VI, VII and plastic. The recent discovery of the latter phase opens a number of relevant questions regarding the microscopic mechanisms determining the thermal conductivity of ice at high pressure, and in particular, the role of hydrogen bonding in thermal transport. A better understanding of thermal transport in ice will be helpful to describe the freezing and melting mechanisms of ice, to advance in the design of cryogenic cooling devices[19], and to understand the properties of ice in the outer space, *e.g.* in comets and

[a] *Department of Chemistry, Imperial College London, SW7 2AZ, London UK*
[*] m.gonzalez12@imperial.ac.uk
[*] fbresme@imperial.ac.uk
‡ Now at Departamento de Química Física I, Universidad Complutense de Madrid, 28040, Madrid ES

moons[20], as well as in the Earth.

In this work we have undertaken a molecular investigation of the thermal conductivity of ice, Ih, VI, VII and the recently proposed plastic phase, using equilibrium and non-equilibrium molecular dynamics simulations. Our study spans a wide range of temperatures and pressures, from standard pressure conditions and the GPa range.Our article is structured as follows. Firstly, we describe the simulation model employed to simulate the ice phases, and the simulation approaches used to compute the thermal conductivity. We use both equilibrium (EMD) and non-equilibrium (NEMD) molecular dynamics simulations. A discussion of our results for the heat flux correlation functions and the thermal conductivities of different ice phases follows. A final section with our main conclusions and final remarks closes the paper.

2 Simulation Details

We performed both equilibrium and non-equilibrium molecular dynamics simulations to compute the thermal conductivity of four types of ice: Ih, VI, VII and plastic phase. The crystallographic structures used in this work for ice Ih, VI, and VII, are shown in Fig. S 1 in the Supplementary information. Most of the simulations were run using the TIP4P/Ice water model, developed by Abascal and Vega.[12] Additional simulations were run with the TIP4P/2005[21] model to simulate the new plastic phase, which has not been computed yet with TIP4P/Ice. TIP4P/2005 is one of the most accurate water models available[22] although the predicted melting point for ice Ih, 252 K, is lower than the experimental value at 1 bar pressure. TIP4P/Ice has been parametrized to reproduce the melting point of Ih[12]. Table 1 collects the force-field parameters for the water models used in this work.

The equilibrium simulations (EMD) were performed using molecular dynamics simulations. The equations of motions were integrated using the velocity-Verlet algorithm[23] with a timestep of 2 fs. For the dispersion interactions we used a cut-off of 0.9 nm, and the electrostatic interactions were computed using the PPPM method[24]. The trajectories were generated using the LAMMPS molecular dynamics programme[25].

The initial configurations were equilibrated in the NPT ensemble for 6 ns, followed by further equilibration in the NVT ensemble for 2 ns. We employed the Nosé-Hoover[26,27] thermostat with a relaxation time of 0.1 ps and the Parrinello-Rahman barostat[28] with a relaxation time of 1 ps. Production runs to calculate the thermal conductivity calculations were performed in the NVE ensemble with a timestep of 1 fs, using trajectories that spanned at least 15 ns. The Green-Kubo (GK) computations were performed using the same approach employed in Ref.[29], which involves the computation of the integral of the heat flux autocorrelation function,

$$\lambda = \frac{V}{3k_B T^2} \int_0^{t_m} dt \left\langle \mathbf{J}_q(t) \cdot \mathbf{J}_q(0) \right\rangle, \qquad (1)$$

where $\mathbf{J}_q$ is the heat flux, V is the volume of the simulation box and t_m is the maximum time used to integrate the correlation function. The heat flux was determined using the microscopic Irving-Kirkwood equation[30],

$$\mathbf{J}_q = \frac{1}{V} \left[\sum_i \mathbf{v}_i e_i + \frac{1}{2} \sum_{i \neq j} \left(\mathbf{f}_{ij} \cdot \mathbf{v}_i \right) \mathbf{r}_{ij} \right], \qquad (2)$$

where e_i and $\mathbf{v}_i$ are the internal energy and velocity of atom i, respectively, $\mathbf{r}_{ij}$ is the distance between i and j, and $\mathbf{f}_{ij}$ is the force between atoms i and j. The maximum time for the integral of the autocorrelation function was set $t_m = 10$ ps. We found that the integrals converge to a stable value in this time interval. Details on the thermodynamic states simulated in this work are compiled in Table 2.

We also performed non-equilibrium molecular dynamics (NEMD) simulations using the approach discussed in Ref.[31]. Two regions with a width of 0.3 nm each, were defined in the simulation cell; one in the middle and another one at the edge of the simulation cell. The molecules in these regions were thermostatted at predefined temperatures. The temperature difference between the hot and cold region was typically 100 K. The equilibrated configurations from the NPT and NVT cycles were used and replicated to generate elongated boxes along the direction of the heat flux, z, in order to construct cells with different lengths. The length of the simulation cell in the z direction varied between $\sim 3-6$ times the length in the, x or y directions. Typical cell lengths varied between $L_z = 8.76$ and 15.33 nm for hexagonal ice, 8.8 and 15.4 nm for ice VI and 8.04 to 14.07 nm for ice VII. Thermal conductivities obtained with different L_z were used to extrapolate the thermal conductivities to the limit, $L \to \infty$, as it is known that the λ in solids might depend significantly on the distance separating the thermostats. The NEMD simulations were run for 10 ns with a timestep of 2 fs.

The starting configuration for hexagonal ice Ih consisted of 432 water molecules and had dimensions $\{x,y,z\}_{Ih} = \{2.67, 2.32, 2.19\}$. The configurations for phases VI and VII consisted of 360 and 432 molecules, respectively, and unit cells,$\{x,y,z\}_{VI} = \{1.81, 1.81, 2.20\}$ and $\{x,y,z\}_{VII} = \{2.01, 2.01, 2.01\}$. The unit cells contained a continuous hydrogen/bonding network, *i.e.* each water molecule was hydrogen bonded to another four neighbouring molecules. Fig. 1 shows radial distribution functions of the hexagonal, VI and VII ice phases for representative thermodynamic states investigated in this work.

3 Results

3.1 Thermal conductivity of ice Ih, VI and VII

We show in Fig. 2 an example of the heat current autocorrelation function (HFAC) and its integral for hexagonal ice Ih at 1 bar and 200 K. The HFAC features significant oscillations at short times $<$ 0.2 ps before the signal decorrelates in about 0.3 ps. The oscillatory behaviour is expected for solids, and it is consistent with previous computations with the TIP4P model for this ice phase[18].

Our thermal conductivity data for the different ice phases for temperatures from 100 to 265 K and pressures from 1 to 20 GPa are collected in Table 2. The thermodynamic states investigated in this work are represented in the phase diagrams shown in Fig. 3 and Fig. 5. Our thermal conductivities for TIP4P/Ice Ih at 200 K and 1 bar, $\lambda = 1.29 \pm 0.06$ W/(K m), which underestimates significantly the thermal conductivity of hexagonal ice[14,32]

Table 1 Force field parameters for TIP4P/2005 and TIP4P/Ice. These 4 site potentials consists of one oxygen atom, two hydrogen atoms, and a virtual particle (M), where the negative charge is located. The particle M is located along the direction of the dipole moment in the HOH plane. See references [12,21] for further details.

Water Model	σ (nm)	ε (kJ mol^{-1})	d(O-H) (nm)	d(O-M) (nm)	q_H (e)	q_M (e)	θ(HOH) (degree)
TIP4P/2005	0.31589	0.7749	0.09572	0.01546	+0.5564	-1.1128	104.52
TIP4P/Ice	0.31668	0.8822	0.09572	0.01577	+0.5897	-1.1794	104.52

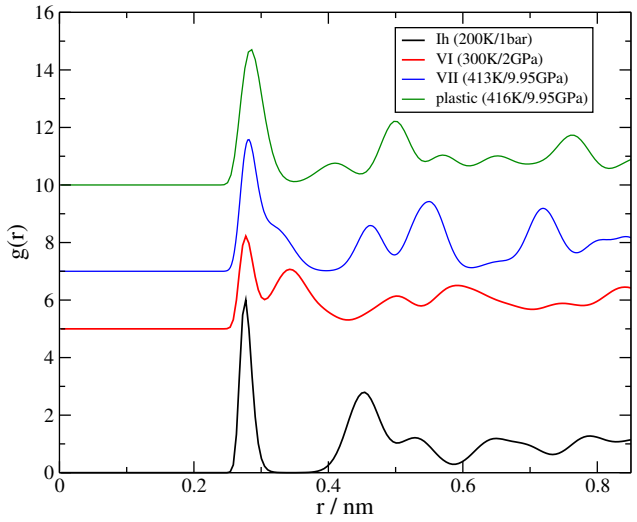

Fig. 1 Oxygen-oxygen radial distribution functions of ice Ih, VI, VII and plastic ice investigated in this work. The results were obtained using the TIP4P/Ice water model for Ih and VI, whilst for VII ice and the plastic phase are computed using the TIP4P/2005 model.

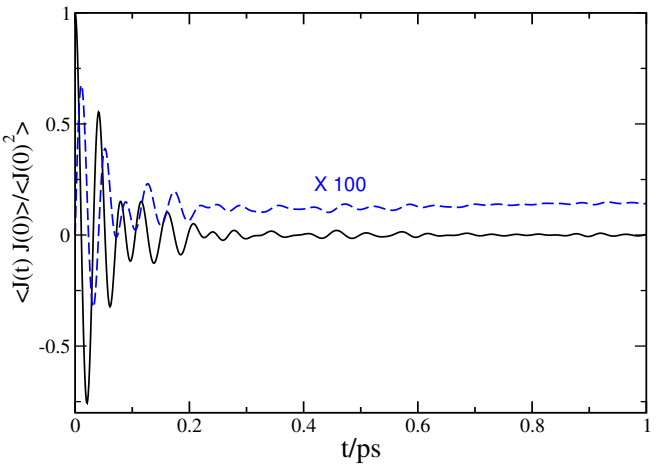

Fig. 2 Normalised heat current autocorrelation function (full lines) and its integral in units of ps (dashed lines, multiplied by 100) for the hexagonal phase of TIP4P/Ice at 200 K and 1 bar.

(See Fig. 3-Bottom). This conclusions agrees with previous simulation studies for this model, $\lambda = 1.19 \pm 0.07$ W/(K m)[33]. We performed additional simulations using the TIP4P/2005 model, which predicts a melting temperature about ∼20 K below the experimental one at 1 bar pressure[34]. The thermal conductivities at 100 K are slightly lower than the ones obtained with the TIP4P/Ice (1.62±0.07 *vs.* 1.85±0.08 W/Km). The result for TIP4P/2005 correlate well with the conductivities we can infer from the interpolations of the TIP4P/Ice data at 120 K, indicating that the deviations between both thermal conductivities might be connected to the lower melting temperature of the TIP4P/2005 model (∼ 20 K lower than that of TIP4P/Ice).

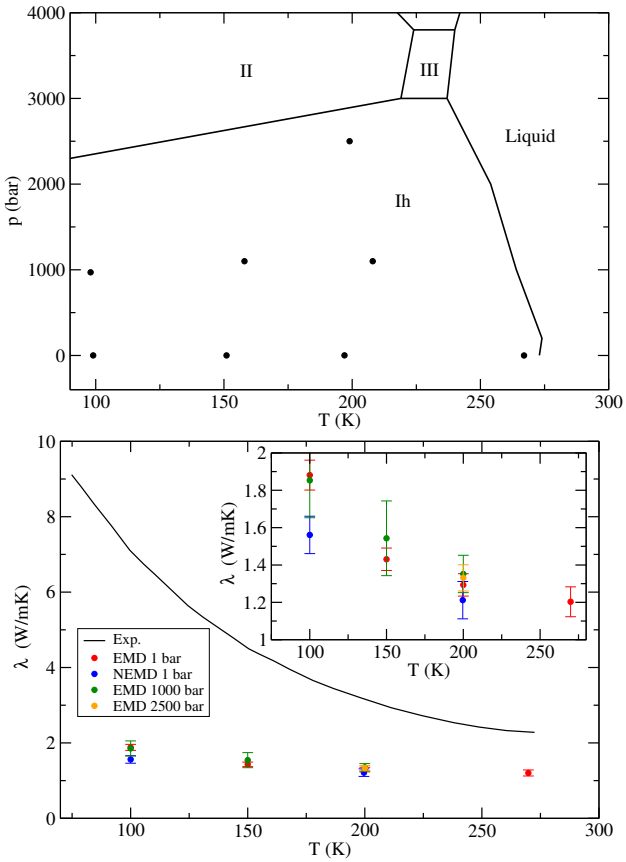

Fig. 3 (Top) The TIP4P/Ice phase diagram[12] around the hexagonal phase. The black dots represent thermodynamic states computed in this work. (Bottom) Dependence of the experimental[32] and simulated thermal conductivities with temperature and 1 bar pressure. Equilibrium and non-equilibrium results (symbols) are shown. The inset shows a detailed view of the EMD and NEMD results. All the computations were performed with the TIP4P/Ice model.

Our results along with those reported before by different authors show that classical, non-polarisable, rigid models underestimate significantly the thermal conductivity, λ, of ice Ih. Previous studies showed that λ of Silicon increases with the size of the simulation cell[35]. To analyze the finite size effects in ice, we performed additional simulations at 100 K increasing systematically the supercell size to 3456 and 11664 water molecules, which corresponds to an increase of the length length of the simulation cell by $(2 \times 2 \times 2)$ and $(3 \times 3 \times 3)$ times, respectively, the original size. The new thermal conductivities are similar to the ones obtained above for the smaller box, $\lambda_{2\times2\times2} = 1.90 \pm 0.05$ W/Km and

Table 2 Thermal conductivity of ice (Ih, VI, VII) at different thermodynamic conditions. All the conductivities (λ_{EMD}) were calculated using the Green-Kubo approach and the TIP4P/Ice model. *ave* refers to the average value obtained for a specific property in the NVE simulations.

Ice Phase	T_{ave} (K)	ρ (g cm^{-3})	p_{ave} (GPa)	λ_{EMD} (W/mK)
Ih	99 ± 2	0.928	0.0049 ± 0.0002	1.88 ± 0.08
	151 ± 4	0.922	0.0024 ± 0.0001	1.43 ± 0.06
	197 ± 5	0.916	0.0073 ± 0.0003	1.29 ± 0.06
	267 ± 4	0.906	-0.0050 ± 0.0005	1.22 ± 0.07
	98 ± 2	0.933	0.097 ± 0.004	1.85 ± 0.08
	158 ± 4	0.929	0.11 ± 0.005	1.54 ± 0.07
	208 ± 5	0.923	0.11 ± 0.005	1.39 ± 0.06
	199 ± 5	0.932	0.25 ± 0.004	1.33 ± 0.06
VI	300 ± 6	1.376	2.17 ± 0.08	1.79 ± 0.08
	298 ± 6	1.334	0.96 ± 0.04	1.69 ± 0.08
VII	302 ± 8	1.688	7.52 ± 0.7	4.6 ± 0.3
	316 ± 7	1.748	9.97 ± 1.9	5.7 ± 0.3
	306 ± 7	1.915	19.75 ± 3.9	9.85 ± 0.4

$\lambda_{3\times3\times3} = 2.08 \pm 0.1$ W/K m. We found a weak dependence of λ with system size. The values of λ in the three orthogonal directions are also very similar $\lambda_{x,3\times3\times3} = 2.03$ W/Km, $\lambda_{y,3\times3\times3} = 2.00$ W/Km, $\lambda_{z,3\times3\times3} = 2.21$ W/Km. A small dependence for these three components is expected since the hexagonal crystal structure does not feature significant anisotropy in terms of the average oxygen-oxygen distances along different directions[36].

To analyse further the accuracy of the TIP4P/Ice model, we performed additional computations of the thermal conductivity of ice Ih using non-equilibrium molecular dynamics (NEMD). We performed NEMD simulations varying the box length along the direction of the heat flux. The thermal conductivities were obtained from the slope of the temperature profile around the temperature of interest in the simulation box, either 100 or 200 K and using the Fourier's law, $J_q = -\lambda \nabla T$, where J_q is the heat flux, which we obtained from the continuity equation (see *e.g.*ref.[10]). The thermal conductivity of solids obtained from NEMD features a significant dependence with the simulation cell size, since the thermostatted slabs influence the mean free path of the phonons. This perturbation results in a decreases of the thermal conductivity with the distance between the thermostats. Such dependence was reported in previous NEMD studies of silicon and diamond[35]. Our results (see Figure 4) reproduce the linear dependence derived before[37],

$$\frac{1}{\lambda(L_z)} \propto \left(\frac{1}{\lambda_\infty} + \frac{4}{L_z}\right), \qquad (3)$$

where the factor of 4 takes into account the average distance of the phonons from the hot to the cold slabs, and λ_∞ is the thermal conductivity of the infinite system. The results for hexagonal ice at 1 bar and 100 and 200 K, can be fitted using Eq. (3), and an estimate of λ_∞ can be obtained. The extrapolated values for the non-equilibrium thermal conductivities, $\lambda_{NEMD} \equiv \lambda_\infty$, are collected in Table 3. We obtain good agreement between the GK and NEMD routes, with slightly lower values for the NEMD results, between 7 and 12% lower. Similar differences have been observed before in simulation studies of argon and silicon[38]. For argon the extrapolated NEMD thermal conductivity agrees with the GK result whereas for silicon it is about half of the GK result between 500 and 1000 K. It was concluded that the extrapolation method discussed above (equation (3)) is accurate when the system size employed is larger than the longest mean free path of the phonon determining the thermal transport. The agreement of our GK and NEMD calculations would therefore indicate that the system sizes considered here are large enough. This conclusion is supported by weak size dependence of the thermal conductivity obtained with GK (see above).

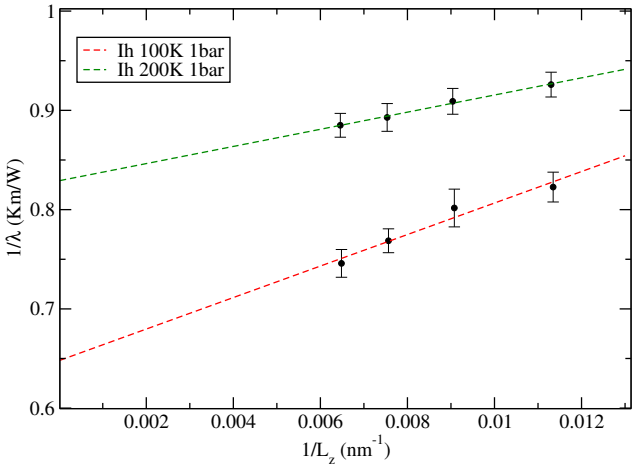

Fig. 4 Dependence of the thermal conductivity (obtained using NEMD) with the length of the simulation box in the direction of the heat flux, L_z. The thermostats are located at 0 and $L_z/2$. The simulations were performed at 1 bar average pressure using the TIP4P/Ice model.

The decay of the thermal conductivity of TIP4P/Ice with temperature is consistent with experimental observations, $\lambda \propto T^{-\alpha}$ (see Fig. 3 and inset in that figure). The decay is often interpreted as an indication of Umklapp scattering processes, where the mean free path varies with T^{-1}, a dependence that is observed in the thermal conductivity too[14]. For hexagonal ice the experimental exponent α is very close to 1[14,36]. The unweighted fit to our data gives an exponent $\alpha = 0.5 \pm 0.1$, significantly lower than the one observed in experiments. Instead, this exponent is similar to the one found in ice V, VI as well as low-density amorphous ices. The exponent obtained here indicates that the TIP4P/Ice model might include additional structural scattering effects, which could be responsible for the lower thermal conductivity observed in the simulations.

The large discrepancies between the simulated and experimen-

Table 3 Thermal conductivities obtained using NEMD and EMD methods. All the data were obtained with the TIP4P/Ice model.

Phase	T (K)	T_{hot}	T_{col}	p(GPa)	λ_{NEMD}(W/mK)	λ_{EMD}(W/mK)
Ih	100	150	50	0.001	1.6±0.1	1.88 ± 0.08
Ih	200	250	150	0.001	1.2±0.1	1.29 ± 0.06
VI	300	350	250	2	1.6±0.1	1.79 ± 0.08
VII	316	350	250	10	5.2±0.3	5.7 ± 0.3

tal results at low temperatures can be addressed by considering the thermal expansion. Analysis of simulation data of TIP4P/Ice reported before[39], shows that the thermal expansion at <200 K departs significantly from the experimental data. At 100 K and 150 K the thermal expansion for Ih ice is overestimated by ∼200% and ∼70%, respectively. This large discrepancy in thermal expansions, indicates that the TIP4P/Ice model might be too anharmonic. This conclusion is consistent with the much lower thermal conductivity observed in the simulations at low temperatures.

The thermal conductivity of most solids increases with pressure. Hexagonal ice, Ih, is an exception[14] to this rule, and it features the opposite behaviour[14]. At 130 K, the experimental thermal conductivity varies from 5 to 4 W/(K m) upon and increase in the pressure of 0.5 GPa[14]. To test this physical behaviour in TIP4P/Ice we performed simulations at 0.11 and 0.25 GPa (see Table 2). In going from 1 bar pressure and 197 K to 0.11 GPa and 208 K the thermal conductivity increases only slightly, from 1.29±0.06 to 1.39±0.06 W/(K m). The difference between these two values is within the statistical error of our computations. Increasing the pressure further to 0.25 GPa and 199 K we get 1.33±0.05 W/(K m), with the difference again within the error of our computations. The same trends are reproduced at temperatures close to the experiments, 151-158 K (see Table 2). From 151 K and ∼ 1 bar to 158 K and 0.11 GPa, the thermal conductivity changes from 1.43±0.06 to 1.54±0.06. Again all these changes are within the error of our computations, and we do not observe a clear dependence of the thermal conductivity with pressure.

We have discussed above the thermal conductivity of the hexagonal phase of TIP4P/Ice. We consider now the thermal conductivity of two high pressure phases, TIP4P/Ice VI and VII, which are stable in the GPa pressure range. We show in Fig. 5-top the phase diagram of TIP4P/Ice including the VII-plastic coexistence line taken from the TIP4P/2005 model, since the full phase diagram for TIP4P/Ice at high pressures has not been determined before. The radial distributions function of ice VI (see Figure 1) at 2 GPa and 300K (TIP4P/Ice as water model), and ice VII at 9.95 GPa and 413 K (TIP4P/2005 as water model), obtained from simulations spanning 10 ns agree with previous studies of TIP4P/2005[40], hence supporting the existence of these phases at the temperature and density indicated in the phase diagram (Fig. 5-top).

Fig. 5 and Tables 2 and 3 collect our results for the thermal conductivities of ice VI and VII at 300 K and at different pressures. Whilst the results for the hexagonal phase show a large underestimation, the computed thermal conductivity for phase VI are in excellent agreement with experiment. Increasing the pressure promotes the transition from ice VI to ice VII. Experimentally, it is known that the thermal conductivity of ice VII is much higher than ice VI (see Fig. 5-middle). The pressure dependence of the thermal conductivity of ice VII has been described before using the Leibfried-Schlöman (LS) equation, which reproduces the experimental observations within 20%[16] accuracy,

$$\lambda = f\frac{V^{1/3}\omega_D^3}{\gamma^2 T} \tag{4}$$

where V, ω_D and γ represent the volume, the Debye frequency and the Grüneisen parameter, respectively, and f is a pressure dependent parameter. Assuming that V, γ, and the Poisson ratio and elastic anisotropy are independent of pressure, Chen et al.[16] derived the following equation,

$$\lambda = A\beta^{3/2} \tag{5}$$

where A is a constant and β is the isothermal bulk modulus defined above. The experimental data for ice VII have been fitted to Eq. (4) in Ref.[16]. We reproduce these results in Fig. 5-middle, for comparison with our simulation data. The thermal conductivity obtained with TIP4P/Ice replicates the increase of thermal conductivity observed experimentally, although the simulation data underestimate the experimental results by ∼30%. Additional simulations using the NEMD approach at 10 GPa confirm the order of magnitude of the thermal conductivity of TIP4P/Ice VII. The lower value of λ observed in TIP4P/Ice VII could be connected to the inaccuracy of the simulation model to reproduce the density of the solid. Examination of previous computations indicates that indeed TIP4P/Ice underestimates the density by about 5%. We have performed additional simulations in the pressure range relevant to our work (see Fig. 5) and we confirm there is a consistent underestimation of the density. Hence, we expect that the lower thermal conductivities obtained in the simulations might be connected to the lower density predicted by the model. To test this idea, we represent in Fig. 5-middle the dependence of the experimental and simulated thermal conductivities of ice VII but as a function of density instead of pressure. The correlation is now much better supporting the idea that the inaccuracy in predicting the equation of state of ice VII is a key factor that prevents TIP4P/Ice VII from predicting more accurate results. This idea can be tested further by comparing the experimental and simulated densities of ice VI, where the performance of TIP4P/Ice in predicting thermal conductivities is much better. We obtain at 0.95 GPa a density of 1.3486, which compares favourably with the experimental data, 1.3656 g/cm^3 [39], resulting in relative deviation between simulation and experiment of ∼1%. See the Supplementary Information for a similar analysis of ice Ih and VI, where we show the density vs. pressure plots and λ vs. density for these icce phases. Numerical results were taken from Table 2.

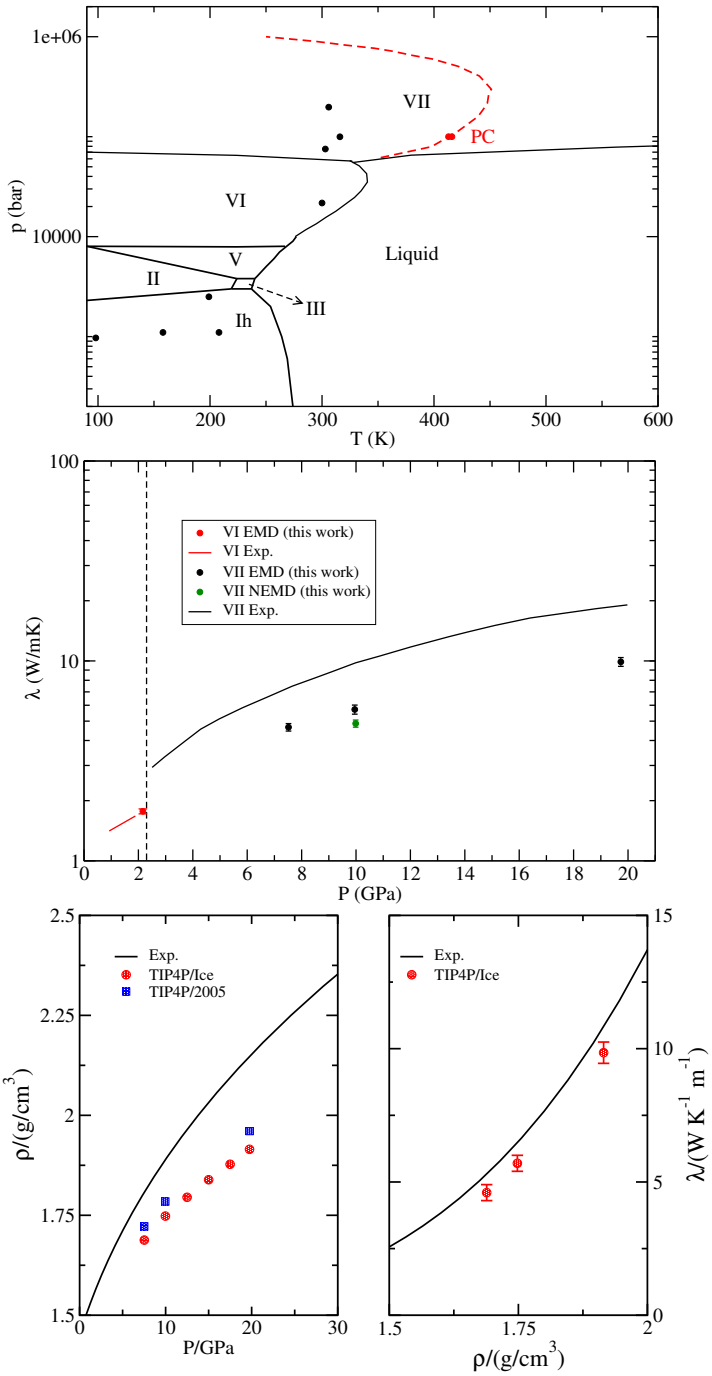

Fig. 5 (Top) TIP4P/Ice phase diagram[12]. The black circles represent the thermodynamic states (pressure and temperature) studied in this work. The dashed red line represents the coexistence line of the VII-Plastic transition for the TIP4P/2005 model[41], and the two points on the line were computed using the TIP4P/2005 model. (Middle) Thermal conductivity of ices VI and VII obtained in this work using the TIP4P/Ice model (symbols). The black and red lines represent the experimental data taken from Ref.[16] and Ref.[15], respectively. The vertical line indicates the coexistence pressure for the ice VI-VII transition. (Bottom-left) Equation of state of TIP4P/Ice VII obtained from experiments (full line using the equation of state in Ref.[42]) and simulations (symbols). (Bottom-right) Dependence of the simulated thermal conductivity with the density for TI4P/Ice VII (symbols) and experimental data (line)[15].

3.2 The Plastic Phase

The plastic phase appears at high pressure, and the water molecules rotate almost freely around their lattice sites. Plastic phases have been predicted using computer simulations and different water models: TIP4P/2005[43], TIP4P, TIP5P[44]. Two plastic phases, with bcc and fcc symmetry were reported using the TIP4P/2005 model. These phases appear at high temperature, >400 K and pressure, >5 GPa[41]. Due to the lack of data for the ice VII-plastic coexistence line using the TIP4P/Ice water model, we decided to perform our analysis using the TIP4P/2005, which is well characterized. We compare in Figure 6 the radial distribution functions of ice VII and plastic ice at 9.95 GPa and 413 and 416 K, respectively. The structures agree very well the with the radial distribution functions reported before.[43] The hydrogen-hydrogen correlation feature a significant reduction of long range order in the plastic phase that is consistent with the emergence of rotational disorder.

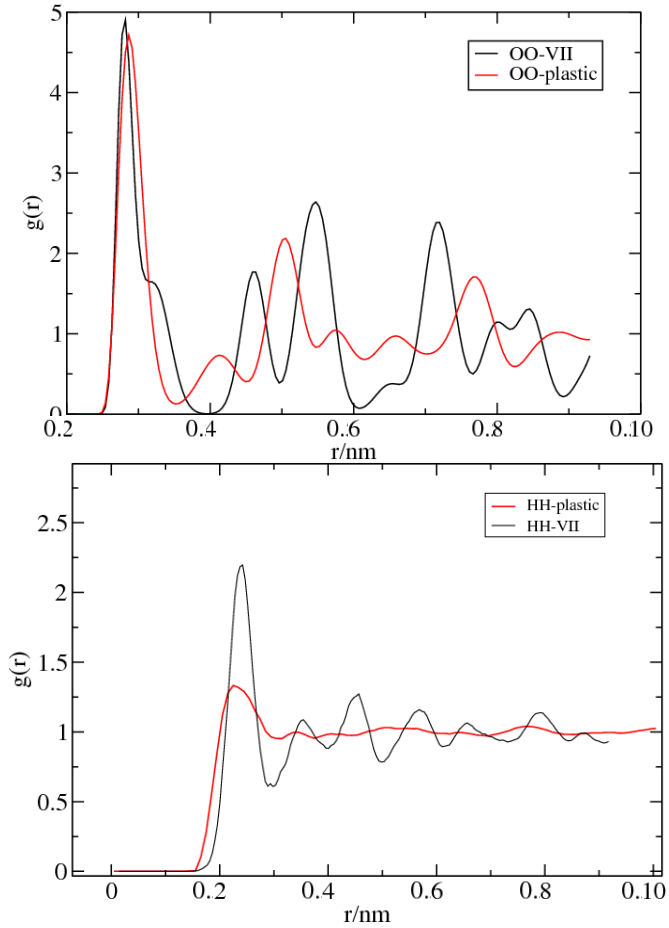

Fig. 6 Radial distribution functions of ice VII at 413 K and 9.95 GPa and the ice plastic phase at 416 K and 9.98 GPa. (Top) Oxygen-oxygen radial distributions function. (Bottom) Hydrogen-hydrogen radial distribution function. All the results were obtained with the TIP4P/2005 model.

To study the correlation between rotational disorder and the heat transport, we computed the thermal conductivity of ice VII and the plastic phase. We chose thermodynamic states close to coexistence (according to the TIP4P/2005 model), namely, ∼415 K

and 9.94 GPa, between. We show in Fig. 7 the heat flux autocorrelation function (HFAF) for the two phases, obtained via simulations in the NVE ensemble. The loss of structural order in the plastic phase translates into a reduction of the oscillations of the HFAF and a shorter correlation time, $\tau = 4.48$ fs as obtained from, $\tau = \int_0^{t_{max}} \left\langle \vec{J}(t)\cdot\vec{J}(0)\right\rangle / \left\langle \vec{J}(0)\cdot\vec{J}(0)\right\rangle dt$, where $t_{max} = 400$ fs. The lack of structure and the shorter correlation time for the HFAF must be reflected in the individual dynamics of the molecules too. To analyse this we computed the velocity autocorrelation function (VAF) of oxygen and hydrogen atoms (see Fig. 7). The VAF of hydrogen decays significantly faster in plastic phase than in ice VII. This result is consistent with the free rotation of the water molecules in the plastic phase. The density of states (obtained from Fourier transform of the VAFs) does also feature significant differences between both phases (see Figure 7). The density of states for oxygen features a maximum at consistent with the periodic structure of the oxygen in both lattices. However the density of states for hydrogen in both phases is notably different. The intermediate frequency mode in ice VII, near the librational region (500 cm^{-1}) is associated to the localisation of the hydrogens in the lattice, and it is not present in the plastic phase, due to the rotation of the hydrogen atoms.

One interesting question is whether the different dynamic behaviour of the atoms in the plastic or ice VII lattices results in different thermal conductivities. This question is of interest, as noted above, the hydrogens are delocalised in the plastic phase and therefore the hydrogen bonding network is disrupted. Hence, comparison of the thermal conductivities of these two polymorphs should provide insight into the relevance of hydrogen bonding in determining the heat transport. We report in Table 4 the thermal conductivities obtained from the integration of the HFAF. Despite the large differences between the structures and the dynamics of hydrogen in the two phases, the thermal conductivity of the plastic and ice VII phases are very similar. Hence, our result indicate that the hydrogen bond network is not particularly relevant in determining the heat transfer of the high pressure phases.

4 Conclusions

We have investigated using equilibrium and non-equilibrium molecular dynamics simulations, the thermal conductivity of hexagonal ice, VI, VII and the recently discovered plastic phase of ice, using state of the art forcefields for water, namely TIP4P/Ice and TIP4P/2005. Despite the excellent performance in other properties, these models predict thermal conductivities that are much lower than the experimental ones. The underestimation is particularly critical for ice Ih, with relative errors >70% with respect to the experiment. The low thermal conductivities obtained via the Green-Kubo approach were supported by using non-equilibrium molecular dynamics simulations. The discrepancies between simulation and theory cannot be corrected with models (TIP4P/Ice) that have been fitted to reproduce the experimental melting temperature of ice Ih. Our simulations show that the discrepancies between experimental and simulated thermal conductivities are not connected to finite size effects.

The thermal conductivity of ice Ih decreases with temperature, in agreement with experiments. However the decay follows a $T^{-\alpha}$

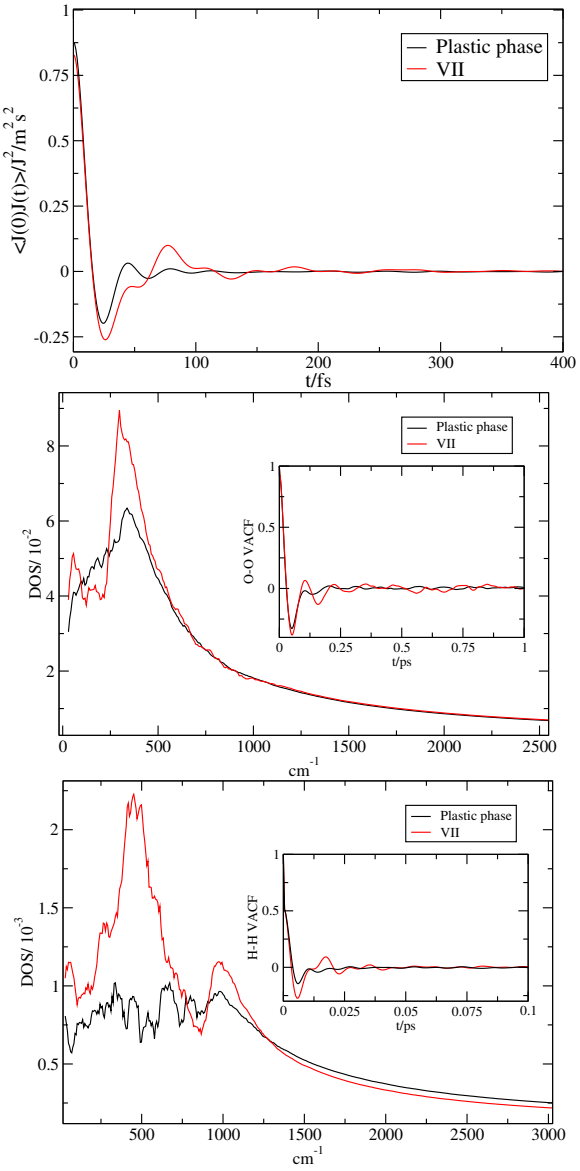

Fig. 7 (Top) Heat flux autocorrelation function of plastic ice at 415 K and 9.94 GPa and ice VII at 410 K and 9.82 GPa. (Middle) Phonon density of states and velocity autocorrelation functions (inset) of the oxygen atoms. (Bottom) Same as middle figure for the hydrogen atoms. All the results were obtained with the TIP4P/2005 model.

dependence with $\alpha < 1$, unlike experimental observations that report $\alpha = 1$ for most solids, including ice Ih. Lower exponents have been reported in amorphous ices, and this suggests that the TIP4P models might incorporate structural scattering defects not present in the experimental ice Ih. Factors that contribute to the inaccuracy of these models are: the lack of quantum nuclear effects, which lead to much higher values of the heat capacity (see e.g. Ref.[45], where the authors used the TIP4PQ/2005 model, to simulate the heat capacities including quantum nuclear effects via path integral simulations), as well as a too large thermal expansion coefficient at low temperatures. The latter factor is significant, since the larger thermal expansion coefficient might indicate that the interactions in TIP4P models are too anharmonic for ice Ih, a conclusion that is consistent with the lower thermal conductivi-

Table 4 Thermal conductivity of the plastic and VII phases. All the results were obtained with the TIP4P/2005 model.

Phase	T_{ave} (K)	ρ_{ave} (g cm^{-3})	p (GPa)	λ_{EMD} (W/mK)
Plastic	415	1.737	9.94	3.9 ± 0.2
VII	410	1.759	9.82	4.1 ± 0.2

ties reported here. Otherwise, the models reproduce the general dependence of the thermal conductivity of ice VII at pressures in the GPa range, although again it is underestimated significantly. The thermal conductivity of ice VI shows good agreement with experiment though. Our analysis indicates that the different predictive behaviour for ice VI and VII can be rationalized using the equation of state (EOS). TIP4P/Ice VI predicts densities for ice VI in good agreement with experiment, while it underestimates the density of ice VII. A rescaling of the thermal conductivity data considering the differences in density between experiment and simulation provides much better agreement between the data of ice VII, indicating a possible route for systematic improvement in the prediction of thermal properties of ice phases at high pressures (GPa range).

A high pressure plastic phase of ice was proposed very recently. This phase coexists with ice VII, but unlike in the latter phase, the water molecules feature orientational disorder in the plastic crystal. We find that the thermal conductivity of ice VII and plastic ice are very similar. This result indicates that the hydrogen bond network does not play a dominant role in the thermal transport mechanism of ice at high pressure.

Improving the agreement of state of the art water models to reproduce thermal transport in ice might require the incorporation of quantum corrections, improvement of the EOS predictions as well as revision of the anharmonicity associated to the pair potential. Despite these deficiencies, the current models reproduce the main physical behaviour of the thermal conductivity regarding temperature and pressure dependence, at high pressures, and predict thermal conductivities for disordered plastic phases similar to those obtain in ordered phases. The latter results awaits experimental verification. This result is of particular interest to advance our understanding of heat transport of ice at high pressures. The extension of these ideas to low pressure polymorphs warrants further study.

5 Acknowledgments

This work has been funded through the EPSRC grant EP/J003859/1. We thank the Imperial College High Performance Service for providing computational resources. We thank Prof. Felix Fernandez-Alonso for interesting discussions.

References

1 G. Hummer and A. Tokmakoff, *J. Chem. Phys.*, 2014, **141**, 1.

2 D. P. Dupont and S. Renzetti, *Environ. Resour. Econ.*, 2001, **18**, 411.

3 D. Eisenberg and W. Kauzmann, *The Structure and Properties of Water*, Oxford Classic Texts in the Physical Sciences, Oxford, 1969.

4 M. L. V. Ramires, C. A. N. de Castro, Y. Nagasaka, A. Nagashima, M. J. Assael and W. A. Wakeham, *J. Phys. Chem. Ref. Data*, 1995, **24**, 1377–1381.

5 M. Zhang, E. Lussetti, L. E. S. de Souza and F. Müller-Plathe, *The Journal of Physical Chemistry B*, 2005, **109**, 15060–15067.

6 F. Bresme, *J. Chem. Phys.*, 2001, **115**, 7564.

7 F. Römer, A. Lervik and F. Bresme, *J. Chem. Phys.*, 2012, **137**, 74503.

8 T. W. Sirk, S. Moore and E. F. Brown, *J. Chem. Phys.*, 2013, **138**, year.

9 F. Bresme, A. Lervik, D. Bedeaux and S. Kjelstrup, *Phys. Rev. Lett.*, 2008, **101**, 020602.

10 I. Iriarte-Carretero, M. A. Gonzalez, J. Armstrong, F. Fernandez-Alonso and F. Bresme, *Phys. Chem. Chem. Phys.*, 2016, **18**, 19894–19901.

11 E. Sanz, C. Vega, J. L. F. Abascal and L. G. MacDowell, *Phys. Rev. Lett.*, 2004, **92**, 255701.

12 J. L. F. Abascal, E. Sanz, R. G. Fernández and C. Vega, *J. Chem. Phys.*, 2005, **122**, 234511.

13 J. L. Aragonés, M. M. Conde, E. G. Noya and C. Vega, *Phys. Chem. Chem. Phys*, 2009, **11**, 543–555.

14 O. Andersson and A. Inaba, *Phys. Chem. Chem. Phys.*, 2005, **7**, 1441.

15 P. A. R.G. Ross and G. Bäckström, *High Temp.-High Press.*, 1977, **9**, 87.

16 D. C. D. T. B. Chen, W.P. Hsieh and J. Li, *Phys. Rev. B*, 2011, **83**, 132301.

17 N. J. English, *Mol. Phys.*, 2008, **106**, 1887.

18 N. J. English, J. S. Tse and D. J. Carey, *Phys. Rev. B*, 2009, **80**, 134306.

19 Y. Rabin, *Cryo. Lett.*, 2000, **21**, 163.

20 J. P. Poirier, C. Sotin and J. Peyronneau, *Nature*, 1981, **292**, 225.

21 J. L. F. Abascal and C. Vega, *J. Chem. Phys.*, 2005, **123**, 234505.

22 C. Vega and J. L. F. Abascal, *Phys. Chem. Chem. Phys.*, 2011, **13**, 19663.

23 L. Verlet, *Phys. Rev.*, 1967, **159**, 98.

24 B. A. Luty and W. van Gunsteren, *J. Phys. Chem.*, 1996, **100**, 2581.

25 S. Plimpton, *J. Comp. Phys.*, 1995, **117**, 1.

26 S. Nosé, *Mol. Phys.*, 1984, **52**, 255.

27 W. G. Hoover, *Phys. Rev. A*, 1985, **31**, 1695.

28 M. Parrinello and A. Rahman, *J. App. Phys.*, 1981, **52**, 7182.

29 F. Bresme, J. Biddle, J. Sengers and M. Anisimov, *J. Chem. Phys.*, 2014, **140**, 161104.

30 J. H. Irving and J. G. Kirkwood, *J. Chem. Phys.*, 1950, **18**, 817–829.

31 J. Armstrong and F. Bresme, *Phys. Rev. E*, 2015, **92**, 060103.

32 N. Ahmad and W. A. Phillips, *Solid State Comm.*, 1987, **63**, 167.

33 N. J. English, J. S. Tse and R. Gallagher, *Phys. Rev. B*, 2010, **82**, 92201.

34 R. García Fernández, J. L. F. Abascal and C. Vega, *J. Chem. Phys.*, 2006, **124**, 1–11.

35 S. Volz and G. Chen, *Phys. Rev. B*, 2000, **61**, 2651–2656.

36 G. A. Slack, *Physical Review B*, 1980.

37 P. K. Schelling, S. R. Phillpot and P. Keblinski, *Phys. Rev. B*, 2002, **65**, 144306.

38 D. P. Sellan, E. S. Landry, J. E. Turney, A. J. H. McGaughey and C. H. Amon, *Phys. Rev. B*, 2010, **81**, 214305.

39 E. G. Noya, C. Menduiña, J. L. Aragonés and C. Vega, *J. Phys. Chem. C*, 2007, **111**, 15877.

40 C. Vega, C. McBride, E. Sanz and J. L. F. Abascal, *Phys. Chem. Chem. Phys.*, 2005, **7**, 1450–1456.

41 J. L. Aragonés and C. Vega, *J. Chem. Phys.*, 2009, **130**, 244504.

42 M. Frank, Y. Fei and J. Hu, *Geochim. Comoschim. Acta*, 2004, **68**, 2781.

43 J. L. Aragonés, M. M. Conde, E. G. Noya and C. Vega, *Phys. Chem. Chem. Phys.*, 2009, **11**, 543.

44 Y. Takii, K. Koga and H. Tanaka, *J. Chem. Phys.*, 2008, **128**, 53122.

45 C. McBride, C. Vega, E. G. Noya, R. Ramirez and L. M. Sese, *J. Chem. Phys.*, 2009, **131**, 024506.